International Journal of Technical Innovation in Modern Engineering & Science (IJTIMES)
Impact Factor: 5.85 (SJIF-2019), e-ISSN: 2455-2585
Volume 5, Issue 12, December-2019

MODELING OF FRACTURE OF STEEL FIBER REINFORCED SELF-COMPACTING CONCRETE

By

VIJAYAKUMAR HALAKATTI*

*Department of Civil Engineering, Smt. Kamala and Shri. Venkappa. M. Agadi College of Engineering and Technology (SKSVMACET) LAKSHMESHWAR-582116, Dist: Gadag, Karnataka State, India
Email:vijayakumar.civil@agadiengcollege.com

Abstract: **- In this paper, a simple, effective and constitutive size dependent finite element based tri-linear model for cohesive fracture of steel fiber reinforced self-compacting concrete (SFRSCC) with two kink points for mode-I fracture is proposed. The co-ordinates of the first kink point is size independent and calculated directly from the geometry of the model whereas for second one the horizontal ordinate is hypothesized to crack tip opening displacement $(CTOD_C)$ of concrete and vertical ordinates is dependent on size of beam. Experimentally, the 3 geometrically similar sizes 100x240x1100,100x120x550 and 100x60x275mm as per RILEM are used for the tests under 3 point bending. The fracture parameters (total fracture energy, initial fracture energy, $CTOD_C$, critical stress intensity factor$K_{IC}$and fracture process zone length c_f) used to link the fracture model are determined by various nonlinear(NLFM) fracture models. The two parameter fracture model, size effect model are based on effective elastic crack approach and work of fracture and crack band model are based on fictitious crack approach. The fracture zone of the model has small aggregate bridging zone and large fiber bridging zone.**

Since the simulated monotonic load (P) v/s crack mouth opening displacement (CMOD) curves perfectly fit with that of experimental curves, a tri-linear model can be predicted by finite element based ATENA software. Unlike for plain concrete, the total fracture energy increases with decrease in size of SFRSCC beams. Hence there is no size effect but noticeable only for large size SFRSCC beams.

The toughness properties such as toughness index, toughness ratio determined as per ASTM C 1018 and ductility ratio increases with decrease in size of beams. Empirical formula established for all these quantities are useful for the design of beams based on toughness and ductility respectively.

Keywords: SFRSCC, tri-linear model, fracture parameters, size effect, toughness, ductility ratio, response reduction factor.

I.INTRODUCTION:

Hillerborg **[1]** initiated the efforts to develop the crack model for fiber reinforced concrete (FRC) and later followed by Naaman [2] and Jun, Zhang, and Victor, C, Li [3].

Hillerborg [1] modeled the fracture process zone (FPZ) as fictitious crack model to analyze the fracture in FRC and determined the fracture energy. The stress-displacement responses were obtained for the bulk material as well as the fracture zone. He suggested that the action of fibers modifies the crack opening behavior and thus controls the stress-displacement response in the fracture zone. The type of fiber (plain, deformed etc.) and fiber material (glass, steel etc.) have an influence on the bond-slip properties of the composite which in turn controls the crack opening behavior.

Visalvanich and A.E. Naaman [2] used the term 'pseudo plastic zone' to describe the zone where fibers provide bridging across cracks. The model proposed assumed that the main portion of energy required during the fracture comes from fiber pullout in the pseudo plastic zone.

Jun Zhang and Victor C Li [3] simulated mode-I crack propagation in FRC by a fracture mechanics approach. A superposition method is applied to calculate the crack tip stress intensity factor (K_{tip}). The model relies on the stress crack width relation as the fundamental relationship to calculate this. There was a very good agreement between the model prediction and experimental load CMOD curves.

Jeffery Roesler et.al [4] extended to develop a tri-linear crack model for fiber reinforced concrete of strength 50 MPa with 40 mm polypropylene (synthetic) fibers under mode –I fracture both by experiments and computer simulation using finite element based ABAQUS software by discrete crack approach. The fracture parameters were evaluated in the laboratory for notched beams made of normal concrete with and without fibers (polypropylene) and tried to link to the proposed model. The usefulness of these fracture parameters in simulating load v/s CMOD curves using ABAQUS software for normal concrete and FRC and later developing crack model by linking the model with fracture parameters were made by them.

They predicted the tri-linear softening model for FRC as shown in **Fig 1** below by simulation using ABAQUS software since the simulation curves were perfectly fitted with those of experimental P-CMOD curves obtained through the 3-point loading tests on three geometrically similar beam specimens as per RILEM recommendations in the laboratory.

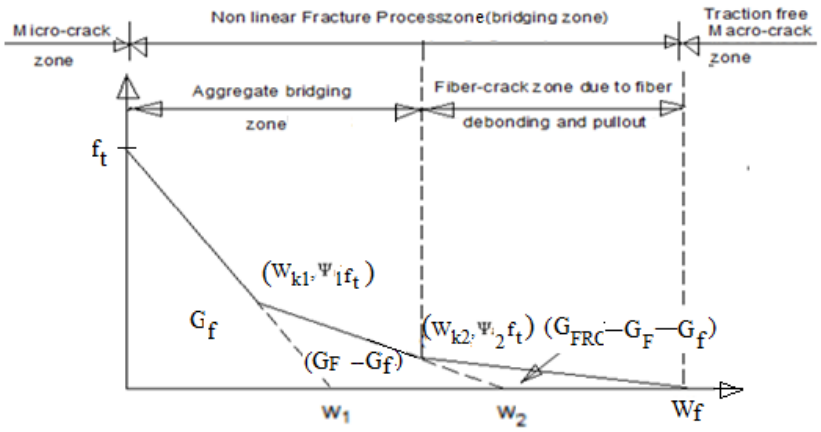

Fig1: Tri-linear fracture model for FRC based on experimental results

The aggregate bridging zone of non-linear fracture process zone of FRC is approximated by the same softening model as that of plain concrete. Since the synthetic fibers do not exhibit the strain hardening property and due to this the split tensile strength of both concrete and FRC are approximately of the same value**,** the fracture parameters f_t, G_F, G_f and $CTOD_c$ determined by using nonlinear fracture models will define the bilinear softening of plain concrete as determined by these investigators [5,6]. The w_2 of FRC is same as that of the final crack width w_f of plain concrete softening model.

The other parameters are total fracture energy (G_{FRC}) which corresponds to the area under the tri-linear softening curve is estimated by the work of fracture method using full load-CMOD curves and the final crack opening width (w_f) of FRC is estimated to be within the range of $\frac{L_f}{4}$ to $\frac{L_f}{2}$ which corresponds to the average pullout length as reported by V.S. Gopalkrishnan and S.P.Shah [7] for randomly distributed fibers.

The fiber bridging zone of FRC represents the concrete material damage at the wider crack opening width. Hence the bilinear softening model developed for concrete is extended as the tri-linear fracture model for the FRC.

Hence, the efforts made by these investigators are considered as a basis to extend it to SFRSCC beams in this investigation, since the self-compacting concrete (SCC) mix is different from normal concrete due to more powder content in it. The SCC is essential in congested formwork with heavy reinforcement due to excellent deformable and segregation resistant property.

Further it is predicted that the presence of steel fibers in SCC will enhance the values of fracture parameters compared that of the SCC. It is investigated by J.Cervenka and Pukl [8] that the steel fibers in normal concrete will reduce the size effect in small size beams due to large amount of fracture energy experienced by them that will transforms the fracture zone into fully plastic zone. Only the largest size shows the size effect due to decrease in the nominal stress σ_{NC} by considerable extent. Hence, these studies are extended to identify the influence of steel fibers in SCC on the size effect.

Further, G. Apparao and B.K.Raghuprasad[9] identified that with a small addition of fraction of steel fibers of length 35 mm, diameter of 0.5 mm and 0.62% by volume in high strength concrete, the mode of failure changes from catastrophic to gradual. The fracture energy is increased by as much as 40 times the plain High Strength Concrete (HSC) with 12.5 mm size aggregates. The length of the tail of the softening portion increases very significantly. Thus, the fracture energy (G_{FRC}) in FRC which is a measure of the ductility decreases as the size of the beam increases.

It is investigated [10,11.12] that steel fibers with hooked ends achieve maximum anchorage with concrete due to its good bond with cement paste thereby increasing the post cracking toughness, energy absorption, ductility, flexural, impact and fatigue strength of concrete. These properties could further increase in SFRSCC due to the compactness of the mix matrix because of higher amount of fine and extra fine filler particles in it. The fibers enable SCC to continue to carry the external loads in presence of large crack widths at post peak condition.

Hence a study of the influence of a specific size (length and aspect ratio) and volume of steel fibers on fracture parameters of SFRSCC beams and their influence on the properties such as toughness and ductility can be made. An investigation is also undertaken to identify the influence of size of SFRSCC beams on toughness and ductility. The toughness and ductility of beams are determined as follows

Frank pap-worth [10] investigated that the area beneath and away from the area of elastic behavior of the load-CMOD graph can be used to measure of the toughness. The toughness can be measured either by USA standard ASTM C1018 or Japanese method JCI-SF4. The ASTM C1018 adopted in this paper introduces toughness index I as the ratio of the absorbed energy up to the given deflection to the absorbed energy up to the first crack '**δ**'. The

toughness indices are I_5, I_{10} *and* I_{30} measured at deflections of 3**δ**, 5.5**δ** and 15.5**δ** respectively as shown in **Fig 2** below. The ratio of these index values to those of SFRC gives comparative values of toughness. However these results cannot be applied as the design value.

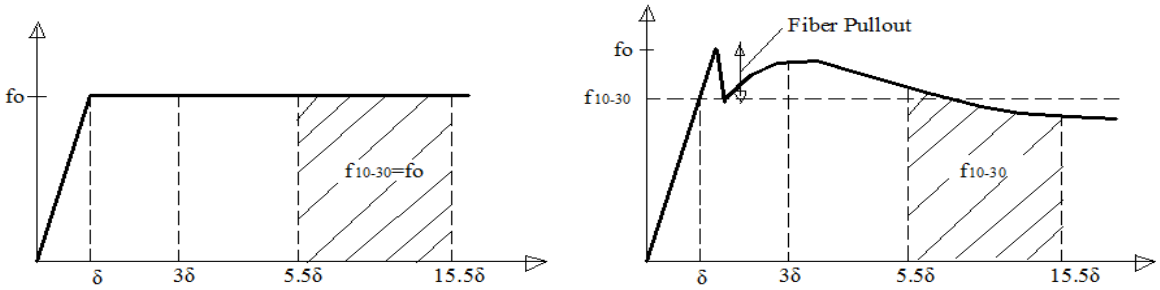

(a) Load deflection curve for elasto plastic composite (b) Load deflection curve for SFRC

Fig 2: Load-deflection curves to measure toughness of SFRC

To overcome this difficulty, a factor known as toughness ratio is introduced and it is given by $R_{a,b} = \left[\frac{100*(I_b-I_a)_{SFRC}}{(I_b-I_a)_{EP}}\right], R_{10-30} = \left[\left(\frac{(I_{30}-I_{10})_{SFRC}}{(I_{30}-I_{10})_{EP}}\right) * 100\right] = 5(I_{30}-I_{10})$ (1)

Where $I_b = I_{30}$ *and* $I_a = I_{10}$ are different toughness indices that can be calculated for both the SFRC and for the perfectly elasto-plastic material and $(I_{30}-I_{10})_{EP} = (30-10) = 20$.

Mean conventional bending stress, $f_{10-30} = \left(\frac{f_o R_{10-30}}{100}\right)$ (2)

Where the f_o is the bending stress at first crack.

$M_{ulti} = \left(\frac{f_{10-30}*Z}{\gamma_m}\right)$ (3)

Where γ_m = factor of safety of the material taken as 1.20 and Z is the section modulus.

Using $f_e = f_{10-30}$ criteria, the flexural members can be economically designed with reduction in thickness up to 25%. It is observed that the accuracy of measurement of I is dependent on the ability to measure **δ** accurately. Any **δ** value more than 0.08 mm is likely to be an error due to machine and operator and should be checked.

From the literature given by Balaguru.P.N [11] that steel fibers make a considerable contribution to ductility by absorbing much more energy before failure compared with plain concrete.

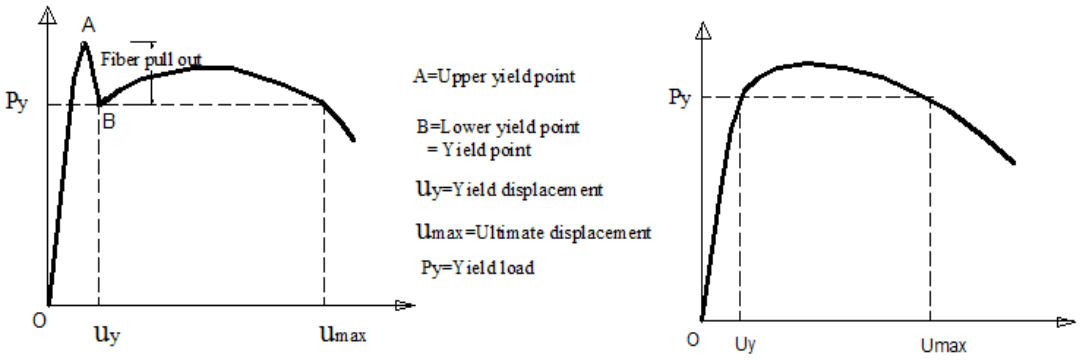

(a) From experimental load CMOD curves (b) From simulation curves

Fig 3: Measurement of ductility ratio using Load-CMOD curves

From the literature given by P. Agarwal and M. Shrikhande[13], the ductility is defined as the capacity of a member or structure to undergo deformation after its initial yield without any significant reduction in yield strength. It is measured in terms of ductility ratio (or ductility factor) which is the ratio of the maximum deformation that an element or structure can undergo without significant loss of initial yielding resistance to the initial yield deformation which is represented in **Fig 3** as shown above.

The ductility is the essential requirement of a structure that must respond to strong ground motion. Some codes assign the value of ductility ratio (μ) from 3-10 to the various structural types. Provision for ductile detailing in the members of reinforced concrete buildings are given in IS 13920:1993. The ductility factor (μ) is used in the reduction of the required linear elastic strength.

The introduction of response reduction factor (R) in base shear formula of IS 1893 code is an attempt to consider the structural ductility. Its numerical value from 1.5 to 5 is assigned to different types of building structures generally on the basis of empirical and semi empirical judgment, experience with building performance in the past earthquakes, experimental and analytical studies.

Hence main contributions of this paper are as follows,

1. To predict the experimental load-CMOD curves through simulation by smeared crack approach suitable for any FRC using finite element based software in which experimental fracture parameters and material

properties are used as input data in it. Simulation is regarded as a virtual tool for testing of beams which avoids the experimental work.

2. A suitable crack model for SFRSCC beams can be proposed by characterizing the experimental load-CMOD curves. Efforts can be made to link the fracture parameters to the proposed model.
3. To identify the influence of enhanced fracture parameters due to steel fibers on the size effect, ductility and toughness of the SFRSCC beams.
4. To identify the influence of size of beam on its ductility and toughness properties.
5. To search for the possibilities to establish size dependent empirical formulas for ductility and toughness based on their experimental numerical results. These formulas can be useful for the design of beams based on toughness and ductility properties respectively.

II. EXPERIMENTAL INVESTIGATION

Mix Proportions for SFRSCC

Based upon the efforts made by the same author in the earlier investigation[14]**, t**he SFRSCC mix is prepared by designing the SCC using Nan Su method[15] for strength 50 MPa using locally available raw materials and this mix is added with the steel fibers at a dosage of 0.6% by the volume of the mix.

The steel fibers conforming to ASTM A 820 are hooked at both ends and are of length 25 mm, diameter- 0.6 mm, aspect ratio- 41.67 and maximum fiber factor (M.F.F)-1.25. The mix proportion is presented in **Table 1** below.

TABLE 1
MIX PROPORTIONS FOR SFRSC CONCRETE

Parameters:P.F−1.12, S/a ratio−5.5	
Material	Qty in $\frac{kg}{m^3}$
Cement	450.00
Fly ash	67.07
Powder	517.07
Fine aggregate	930.6
20mm(20% of CA)	149.04
12.5mm(80% of CA)	596.16
Water	163.263
SP dosage (% of cement)	5.40kg
Steel fibers of length 25mm@ 0.6% by volume of mix	46.8 kg
Ultimate strength of steel wire confirming to ASTM A 820,Type I cold drawn type from mild steel	> 1200 MPa

The tests for workability requirement were conducted on fresh mix as per EFNARC guidelines and the strength tests on hardened mix. These results are given in **Table 2** and **3** respectively.

TABLE 2
PROPERTIES OF FRESH MIX

Properties	**Range**	**Results**
Slump flow	650-800mm	660 mm
T_{50} cm	2—5 sec	3.8 sec
J-ring	0—10mm	6.6 mm
V-funnel	8—12 sec	8.0 sec
V-funnel– (5min)	+3sec	10.1 sec
L-box(H_2/H_1)	0.8 –1.0	0.82
U-box(H_1-H_2)	0—30 mm	28 mm
Orimet	0—5 sec	3.1 sec

TABLE 3
PROPERTIES OF HARDENED CONCRETE

Properties		**IS code reference**	**Results**
Compressive strength	7 days	I.S. 516:1959	41.73 MPa
	28 days		58.67 MPa
Young's modulus			39700MPa
Poisson's ratio			0.186
Split tensile strength		I.S. 5816:1999	4.384 MPa
Post cracking behavior of SFRSCC(Brittle or Ductile)		--	Ductile

Post cracking behavior of SFRSCC in ATENA software	--	SFRC

Testing protocol for three point bending experiments for notched beams

The dimensions of beams as per the RILEM-FMC-50 recommendations are given in **Table 4** below. The span to depth (S/D) ratio is equal to 4, maximum size of coarse aggregate d_a= 20mm, $\frac{(a_o}{D)} = 0.33$. Type of notch in the beams is saw cut using machine.

TABLE 4
BEAM DIMENSIONS IN MM

Beam series	**Span (S)**	**Length (L)**	**Depth (D)**	**Thickness (t)**	**Notch depth(a_o)**
Large-fiber reinforced (L.F. Series)	960	1100	240	100	80
Medium-fiber reinforced (M.F.Series)	480	550	120	100	40
Small-fiber reinforced (S.F. Series)	240	275	60	100	20

The three geometrically similar notched SFRSCC beams are tested in the laboratory under the three points bending using very stiff servo hydraulic deflection controlled machine and clip gauge of 10 mm maximum capacity. The tests are performed under deflection control at prescribed deformation rate of 1micron/sec (0.06mm/min).The experimental fracture parameters of SFRSCC beams are determined using load CMOD curves by applying various nonlinear fracture models applicable to concrete.

(a)Specimens for testing (b) Arrangement of specimen for test (c) Clip gauge in groove

(d)(e)& (f) Cracks in SFRSCC beams captured during tests on different specimens
Fig 4: Different stages of test on the beams

III. SIMULATION

The **c**omputer simulation is a relatively new and robust tool for checking the performance of concrete structures in design and development. Such simulation can be regarded as a virtual tool for testing of building structures under the designed loading and environmental conditions. It can be used to confirm and support the structural solutions with complex details or nontraditional problems and can serve to find an optimal and cost effective design solution. It is a modern tool for optimization of structures thereby achieving economy. Simulation is useful in such cases which are not well covered by the code of practice provisions. Hence nonlinear analysis of concrete structures became a novel design tool. It employs the power of computer simulation to support the structural engineers. The finite element based failure analysis can take the advantages of rational theories such as fracture mechanics. This can be performed by finite element based **ATENA** software in this research.

The theory of fracture mechanics of concrete introduces finite element based software [16] to simulate experimental softening curves by TWO approaches. They are smeared crack approach and discrete crack approach.

The Discrete crack approach is based on cohesive crack model in which crack path is assumed as priori and mesh with cohesive surface elements are arranged so that the path coincides with the boundaries between the bulk elements thereby bridging continuum between these two types of elements. Software available in the market based on this approach are ABAQUS, FRANC and CRACKER.

The Smeared crack approach introduced by Rashid is based on **Bazant**'s crack band model. The width of crack band w_c includes the group of cracks which is several times larger than the aggregate size .It is based on the concept of replacing the crack by a continuous medium with same or altered physical properties. This is adopted where distributed cracking is possible. The crack is not straight but tortuous. To use software by this approach, the given beam specimen is divided with only general linear elastic element known as bulk elements of rectangular shape of suitable size. The disadvantage is of convergence of the solution for decreasing mesh size. The size of mesh cannot be smaller than " w_c ". The bulk element employs two dimensional plain stress assumption to represent the linear elastic behavior in stage-I. Hence these elements have the stress-strain relationship governed by $\sigma_{bulk\ element} = f_{elastic}(\varepsilon)$. Software available in the market based on this approach is ATENA software.

This finite element method (FEM) based computer program SBETA was developed and implemented in ATENA software. The material models in this program are based on damage concept and smeared crack approach. The tensile behavior of concrete is modeled by nonlinear fracture model (NLFM) combined with the crack band theory. In this theory, the smeared crack approach is used for both cracks and reinforcement. Its parameters are tensile strength (f_t), shape of stress crack opening (assumed as exponential in case of concrete) and the total fracture energy (G_F). Hence, the tensile fracture in concrete is based on fracture energy criterion. Cracks are initiated when principal tensile stress exceeds the tensile strength of concrete material. The direction of cracks is normal to the principal tensile stress at the crack initiation.

The main material model implemented in ATENA software developed and optimized for normal concrete can be used also for extra ordinary types of concrete such as high strength concrete, masonry and bricks using appropriate material parameters. Special models with high ductility and suitable function in tension are available for SFRC.

The finite element method (FEM) based ATENA software needs to define the type of tension softening for smeared crack approach as SFRC. The experimental material properties such as Young's modulus (E), Poisson's ratio (μ), Split tensile strength (f_t), Cube compressive strength (f_c) and Specific weight (ρ) of the material and the total fracture energy (G_{FRC}) are used as input data in the software.

The two non-linear solution techniques are such as Standard Newton Raphson and Standard Arc Length methods with iteration of 40. However these can be modified with iteration numbers as required. However in this analysis iteration of 60 are used.

Simulation in the ATENA software is performed using Newton Raphson solution parameter with number of iterations of 40. The load cycles of around 400 to 800 are required. The final crack width is restricted to $w_f = 8.5mm$ which is approximately equal to $\frac{(L_f}{3}$) of the fiber.

Simulation for softening curves is performed for full beam without taking the advantage of symmetry in order to avoid an imposed symmetrical mode of failure with two failure cracks. The mesh is formulated by using four node quadrilateral bulk elements with 10 elements over the depth of beam and of total 1280 nodes and 960 elements for beams of each size by both the approaches. The arrangement of mesh is shown in **Fig 5** below.

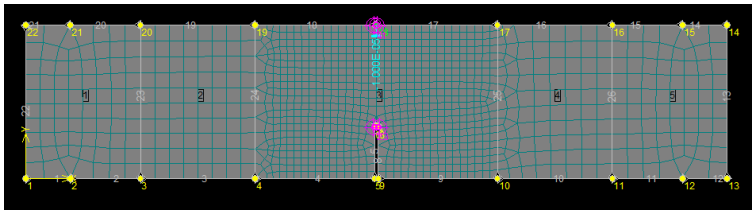

Fig 5: Arrangement of mesh in the beams

IV. RESULTS AND DISCUSSIONS

The simulated load CMOD curves obtained are compared with the experimental load CMOD curves for SFRSCC beams of all the sizes. The softening curves can be predicted by simulation. The combined experimental and simulation curves for large size beams series (L.F. Series), medium size beams (M.F. Series) and small size beams (S.F. Series) are shown in **Fig 6 (a), (b)** and **(c)** respectively.

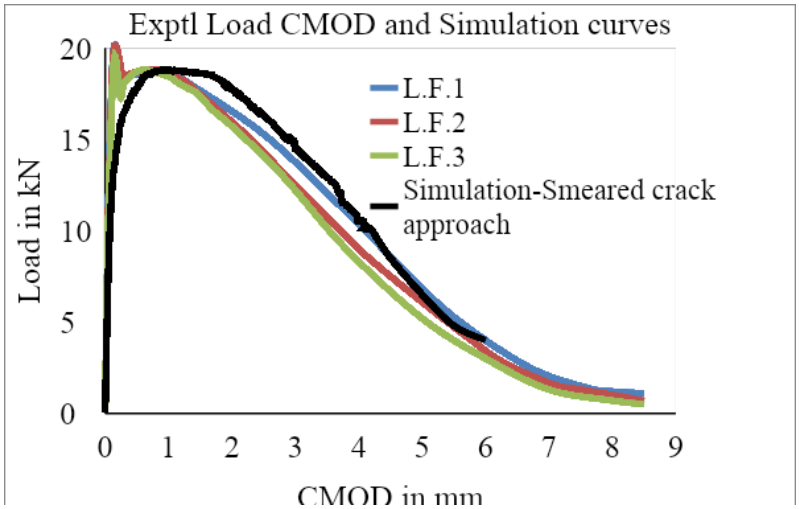

(a)For large size fiber reinforced beam specimens

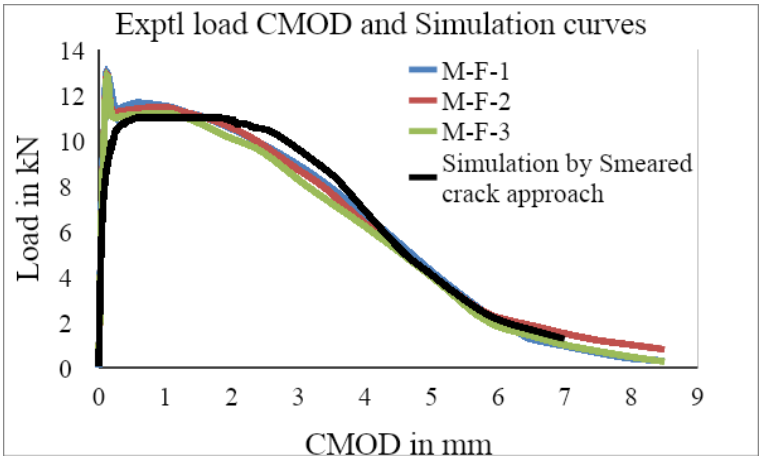

(b)For medium size fiber reinforced beam specimens

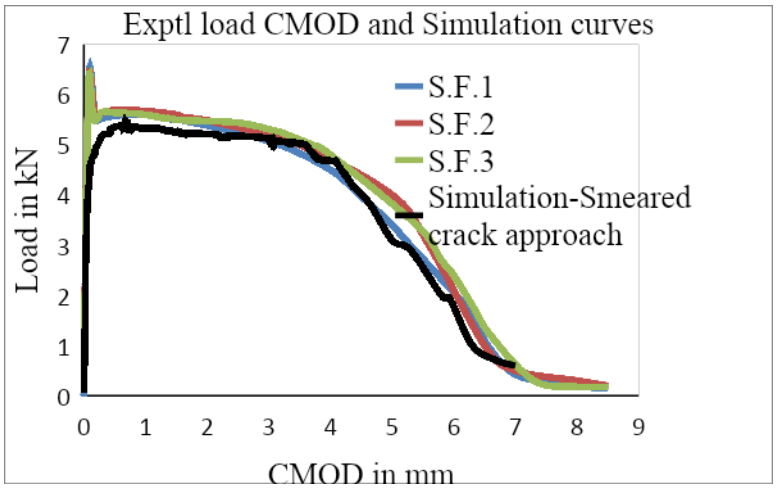

(c) For small size fiber reinforced beam specimens

Fig 6: Experimental and simulation Load-CMOD curves in combination for 3 geometrically similar beams

It is observed from **Fig 6** that there is sudden drop of load in the experimental load-CMOD curves soon after it reaches the first crack load. This drop is known as the fiber pull out. However, it is understand from **literature [11]** that if the dosage of steel fibers is increased, then this drop goes on reduces thereby there will be significant improvement with stable post crack behavior. The SFRSCC is made of two different materials. SCC is brittle and weak material whereas steel fibers are strong and ductile. When such composite material is loaded, the matrix will fracture long before the steel fibers reach its tensile stress. Till then, they pose resistance in combine until it reaches the peak load causing certain deformation in the form of crack width which is CMOD. This part of the load-CMOD curve from zero to maximum load (portion O-A of the curve shown in **Fig 7** below) is known as penalty stiffness.

The failure is initiated by the formation of cracks process zone with micro-cracks in the region of tensile stresses. The crack initiation load (P_{cr})is ranging from 0.50 to 0.60 of peak load(P_u). At peak load, the matrix cracks fully. Once the matrix cracks, there will be sudden drop in load (AA' of curve). But, the composite will continue to resist load that are lower than peak load. The load is transferred from composite to the steel fibers at the crack interface. Hence, further load carrying capacity comes from the fibers transferring the load across the matrix. As the deformation (crack width) increases, fibers tend to pull out of the matrix resulting in lower load carrying capacity. Till this stage, SFRSCC behaves elastically.

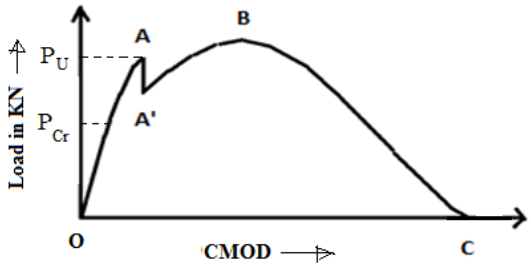

Fig 7: Typical Load-CMOD curve for SFRSCC beams

Later, the fibers start carrying increased loads. Then the composite starts to behave in-elastically (or plastically). The strain hardening property of steel fibers (A'B of curve) contribute until the curve reaches another (second) peak load. There will be increase in the non-linear behavior and will increase the load for increased crack width in the load-CMOD curve up to second peak load. At this stage, there will be the formation of multiple cracking, de-bond and slip of fibers from matrix and it will further continue. As the load is further increased beyond second peak load, the fibers start to pull out of the matrix and the crack reaches its maximum value at zero loads. This is represented (portion BC of curve) by decrease in slope at the tail end of the curve.

The difference between experimental and simulated load-CMOD curves lies with its behavior at first crack (peak) loads. In experimental curves there is sudden of peak load due to phenomenon such as fiber pullout where as in simulated curve this will not occur. Hence, simulation does not provide an accurate prediction in the region of first cracking when compared to test results.

The experimental and simulated load-CMOD curves shown in Fig **6(a),(b)** and **(c)** for individual size of beams are further segregated as experimental load-CMOD curves as shown in **Fig 8(a)** and simulated load CMOD curves as shown in **Fig 8(b)** below.

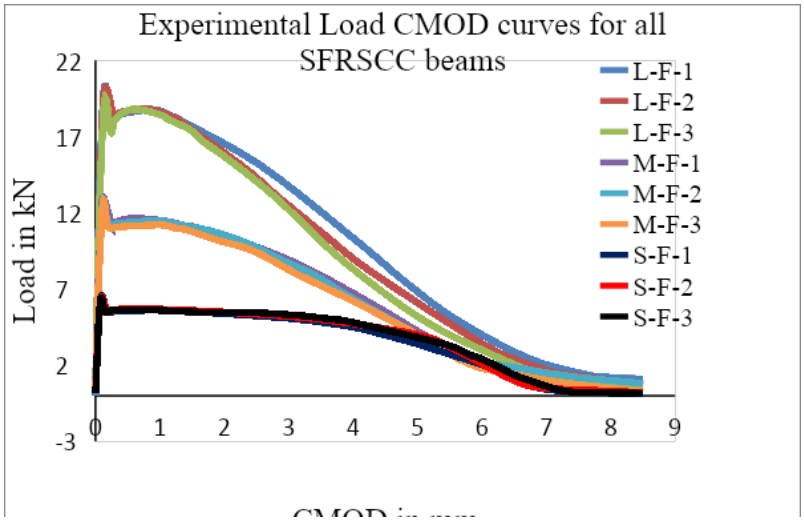

(a) Experimental load-CMOD curves combined for all three geometrically similar size beams

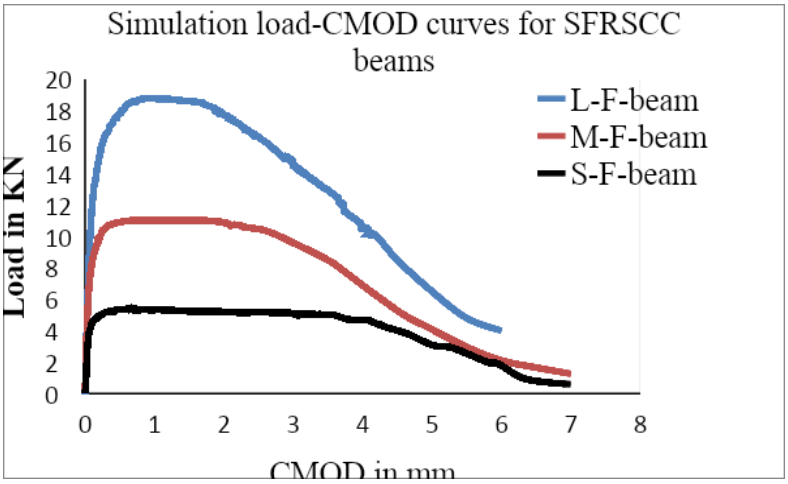

(b) Simulated load-CMOD curves using ATENA software combined for all 3 geometrically similar beams

Fig 8: Load-CMOD curves for all beams

It is observed that all these simulation curves better fit with each other validating the experimental curves except in the region of first crack or peak load. It is also identified that the peaks of load CMOD curves goes on decreasing and tends to become flat as the size of the beam becomes smaller. This indicates that the SFRSCC beams increases its ductility as its size reduces. The decrease in peak loads of smaller beams associated with prolongation of the tail end (or post peak) of the Load-CMOD curve to the maximum extent without decrease in the yield load could be responsible to yield higher fracture energies in smaller beams compared to the larger beams. This behavior indicates the stable crack growth process resembling the ductile behavior of smaller beams thereby increasing their ductility ratio (μ) compared to larger beams. Thus the fracture energy could increases as the size of the beam reduces.

The characteristic length (L_{ch}) given by the relation ($\frac{EG_F}{f_t^2}$) for all beams as calculated in **Table 5** below is extremely large as compared to plain mix beams which indicates that SFRSCC beams are extremely ductile and increases for smaller beams which indicates the increase in ductility of the smaller beams. In case of larger beams, the tail end of the load CMOD curve after peak load will decrease steeply due to its high value of peak load associated with large energy release with unstable crack growth indicating the brittle behavior.

Study of the Crack Pattern in SFRSCC Beams

Using the experimental fracture parameters and material properties as input data in the software, the simulation is performed to obtain load CMOD curves as above. During this process, the crack patterns in the notched beam were captured for all the beams at different load steps and are shown in **Fig 9** below.

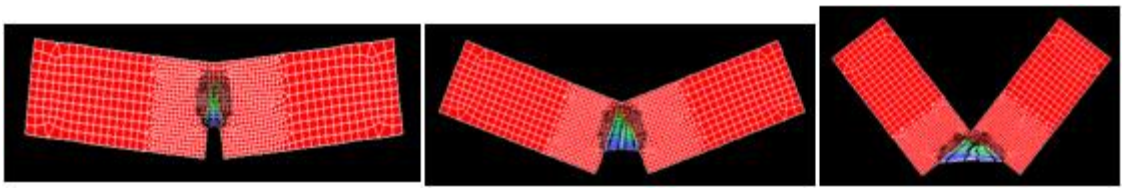

(a) load step no 30 b) load step no 150 c)load step no 400

Fig 9.a: Crack pattern in large notched beam at different load steps

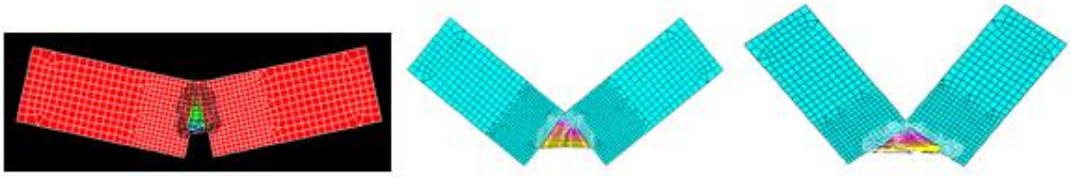

(a) load step no 60 b) load step no 250 c)load step no 500

Fig 9.b: Crack pattern in medium notched beam at different load steps

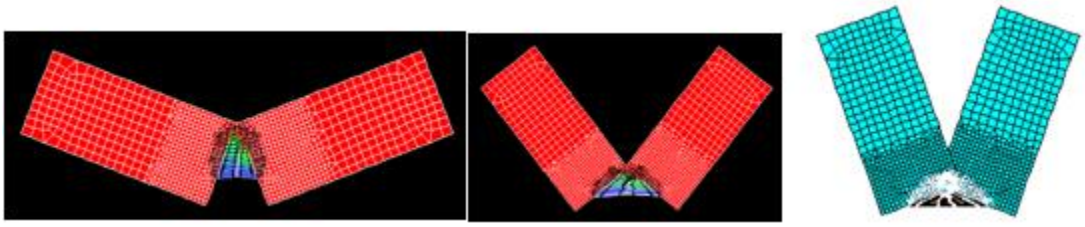

(a) load step no 100 b) load step no 350 c)load step no 700
Fig 9.c: Crack pattern in small notched beam at different load steps

V.EVALUATION OF FRACTURE PARAMETERS FOR SFRSCC

The load-CMOD curves of **Fig 6** or **Fig 8** are used to estimate the G_{FRC} for SFRSCC beams as per the RILEM method of Hillerborg et al. The work of fracture method proposes equation $G_{FRC} = \left[\frac{W_t}{(b-a_o)t}\right] = \left[\frac{W_o+2P_w\delta_o}{(b-a_o)t}\right]$ where $W_o$is the area below load CMOD curves, P_w=self-weight of beam and δ_o= CMOD displacement corresponding to load applied by testing machine $P_a = 0$. The G_{FRC}values determined for all the beams are represented in second column of **Table 5** below.

Utilizing the peak loads of load CMOD curves all size beams, the initial (Specific) fracture energy (G_f) and fracture process length (c_f) are determined as per RILEM method based on the size effect model proposed by Bazant et al.

In absence of at least one loading and unloading cycle in load-CMOD curves, the $CTOD_c$ given by two parameter fracture model (TPFM) of Jenq and Shah [16] can be obtained for SFRSCC from using the relation $\sqrt{(\frac{32G_fc_f}{E\pi})}$ as established by Bazant et al.[16]. which is applicable for beams with depth of the notch (a_o) $\gg$ (c_f). The a_o for larger beam is 80 mm and c_f is 88.45mm. However, a unique value of $CTOD_c$ for SFRSCC beams is calculated from above expression using experimental results and is useful to identify the possibilities to link this parameter to the proposed tri-linear model for the SFRSCC beams.

To determine the experimental fracture process length (c_f) , the average of the peak loads (P_j) for all 3 geometrically similar beams from corresponding load v/s CMOD are to be used to calculate (P_j^o) which includes self-weights of the beams using the relation $\left[P_j^o = \left(P_j + \left(\frac{2S_j-L_j}{2S_j}\right)gm_j\right)\right]$,where gm_j represents the self-weight of each beam.

A graph is developed between $X_j v/s Y_j$. In this graph, the horizontal co-ordinate indicates the parameter X which is used to indicate the each size of 3 geometrically similar beams.

Thus, X_j= $X_{1,2,3}$, where, X_1= D_1=240mm, X_2 = D_2=120mm and X_3= D_3= 60 mm

The Y is the vertical ordinate which represents the corresponding values determined using the corresponding values in the formula $(\frac{Dt}{P_j^o})^2$ where D=depth of corresponding beam, t = thickness of beam 100mm and is constant for all three beams and P_j^o=corrected maximum load for each beam.

If, Y_j= $Y_{1,2,3}$, then, Y_1= Y value for larger beam ,Y_2= Y value for medium beam and Y_3= Y value for smaller beam.

Using the linear regression line of the form $Y = (A_BX + C_B)$ of the graph, where A_B= slope of line and C_B is the initial intercept, the A_B and C_B are evaluated. The fracture process length (c_f) is determined using the relation, $c_f = \left[\left(\frac{g(\propto_o)}{g'(\propto_o)}\right)\left(\frac{C_B}{A_B}\right)\right]$. The $g(\propto_o) = g\left(\frac{a_o}{D}\right)$ is geometric factor and $g'(\propto_o)$ is its first derivative for $\frac{(S}{D}) = 4$ at initial notch $a = a_o$.

With similar procedure, simulated c_f can be evaluated using the peak load of simulated load-CMOD curves.
These results are presented in **Table 5** below.

It is known that the fracture energy is dependent on many factors such as experimental errors caused due to testing equipment and setup and dissipation of energy in specimen bulk. The other major difficulties in capturing the tail part of the curves especially for smaller beams causes the fracture energy of SCC beam as size dependent instead of material dependent property.

It is known that the fracture energy is dependent on many factors such as experimental errors caused due to testing equipment and setup and dissipation of energy in specimen bulk. The other major difficulties in capturing the tail part of the curves especially for smaller beams causes the fracture energy of SCC beam as size dependent instead of material dependent property.

TABLE 5
FRACTURE PARAMETERS OF SFRSCC

Beam ID	G_{FRC} **in N/m**	**CV in %**	L_{ch} **av** $= \frac{EG_F}{f_t^2}$ **In m**	$(G_f)_{Exp}$ **In N/m**	$(G_f)_{Sim}$ **In N/m**	**% error**	c_f **Exptl (mm)**	c_f **Simln (mm)**	**% error**	$CTOD_c$ **Exptl (mm)**	$CTOD_c$ **Simln (mm)**	**% error**
L.F.1	5748.2	2.81	115.03									
L.F.2	5498.9											
L.F.3	5460.0											
M.F.1	6684.5	2.14	136.79									
M.F.2	6721.5											
M.F.3	6460.1			418.3	425.8	1.78	88.45	115.2	30.3	0.098	0.11	12.8
S.F.1	7373.1	3.58	158.65									
S.F.2	7767.0											
S.F.3	7901.9											

It is known that the fracture energy is dependent on many factors such as experimental errors caused due to testing equipment and setup and dissipation of energy in specimen bulk. The other major difficulties in capturing the tail part of the curves especially for smaller beams causes the fracture energy of SCC beam as size dependent instead of material dependent property.

The total fracture energy for SCC and SFRSCC beams can be determined by both load-CMOD and load-deflection curves. RILEM recommends determining the total fracture energy of concrete based load-line displacement curves. This is truly essential as per RILEM requirement and also for un-notched beams. It is identified [9] that the fracture energy calculated using TPB specimens from Load v/s Deflection curves includes the errors associated with crushing of support, load points and significant dissipation of energy in the bulk of concrete under highly stressed zones.

To avoid these errors, the fracture energy is determined using Load-CMOD curves. This is because the errors involved in the calculation of fracture energy are less if load-CMOD curves are used due to absence of possible errors from supports crushing and other sources. The energy calculated can be considered as true fracture energy of concrete. Many investigators preferred to use the terminology total fracture energy based on load-CMOD curve even-though it is not true according RILEM. In this research, the evaluation of G_F based on load-CMOD is emphasized. This is due to the provision to mount the clip gauges in the notches properly. This will ensure the stable and accurate measurement of CMOD (crack width) values rather than deflection which leads errors due to above reasons at the increased loads in the tests.

Further, the post peak behavior which determines its fracture energy of SFRSCC beams depends on characteristics, quantity, distribution in the matrix and orientation of fibers with regard to the crack plane. It also depends on the quality of the cementitious matrix surrounding the fibers. Although, it is hard to identify the influence of fiber orientation and distribution on fracture energy, but other factors definitely will change the post peak behavior. However, in this research, the type and quantity of steel fibers used in all SFRSCC beams is same. Hence, the above factors do not influence fracture energy of SFRSCC beams.

Thus, the total fracture energy of SFRSCC beams using load-CMOD curves are considered as true values and can be related to the corresponding geometry (depth) of the beams.

The G_{FRC} values of the **Table 5** are used to develop a graph showing its variation with depth of beams. This graph is developed as shown in **Fig 10** below. Using this graph, the G_{FRC} for any intermediate beam of depth 60 to 240 mm can be directly evaluated. However, this problem is simplified assuming arbitrarily that the G_{FRC} varies linearly within this range of beams, a linear regression line equation is established as follows,

$$G_{FRC} = [7600 - 12.22(D - 60)] \text{ N/m} \quad (4)$$

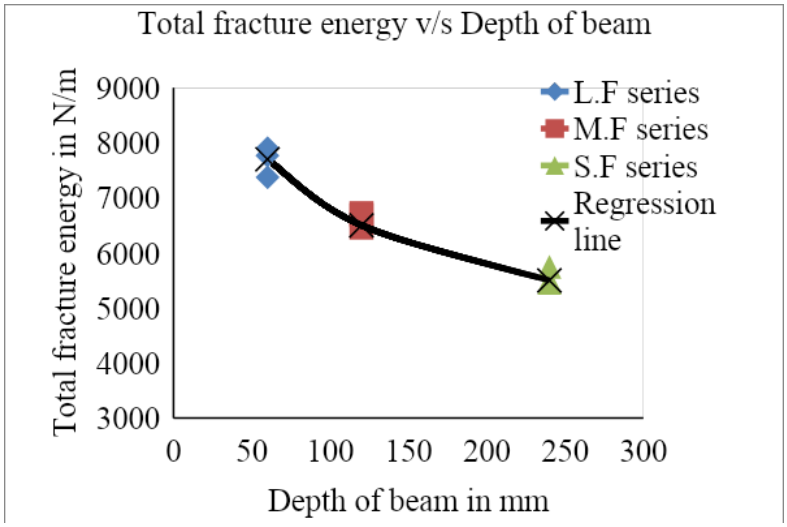

Fig 10: Graph showing the variation of G_{FRC} of beams with depth

The fracture parameters for SFRSCC as given in the above **Table 5** are compared with those of SCC. These fracture parameters for SCC as determined by the same author [17] in the earlier investigation are represented in **Table 6** below.

TABLE 6
FRACTURE PARAMETERS OF SCC FROM EXPERIMENT

Beam series	**Average peak load in kN**	**Mean of G_F in N/m**	$(G_f)_{Exp}$ **in N/m**	**Fracture process length (c_f)in mm**	**Average $CTOD_c$in mm**
L.P	12.281	288.80	86.33	18.72	0.0146
M.P	8.866	248.49			0.0116
S.P	6.289	221.83			0.0079

It is observed from **Table 5** that the ratio of $(\frac{G_{FRC}}{G_f)}$ for SFRSCC from experiments varies from 13.31 for L.F series to 15.83 for M. F. series and then to 18.36 for S.F series with the minimum co-efficient of variation whereas for SCC referred from **Table 6**, the ratio $(\frac{G_F}{G_f})$ varies from 3.35 for L.P series to 2.87 for M.P series and 2.56 for S.P series.

Referring the values of above **Table 5** and the results evaluated from the earlier investigations by the author [17] as given in **Table 6,** it is learnt that the total fracture energies G_{FRC} of SFRSCC beams are many times higher than G_F of SCC beams. The ratio of average G_{FRC} to G_F for larger beam series is 19.28 and increases to 26.65 for medium beam series and 34.63 for smaller beam series. This ratio systematically increases as the size of the beam reduces.

For SCC, the G_F decreases as the size of beam reduce whereas for SFRSCC, the G_{FRC} increases as the size of the beam reduce and both are the size dependent properties. This behavior of variation of G_{FRC} in SFRSCC beams is similar to that investigated by G. Apparao and B.K. Raghu Prasad [9] for FRC. This is due to the presence of steel fibers in SFRSCC which is responsible to prolong and extend the tail end (post peak portion) of load CMOD curve with loads higher than the yield load for small beam compared to large beam. The extension of CMOD with loads greater than their corresponding yield loads increases towards the tail end (post peak crack behavior) of the curve considerably for smaller beams as compared to larger beams.

It is observed from **Fig 6** that the post peak portion of load-CMOD curve of larger beam shown in **Fig 6(a)** are steeper than that of medium and small size beams shown in **Fig 6(b)** and **Fig 6(c)** respectively. Similarly the post peak portion of load-CMOD curve of medium size beam is steeper than smaller beams. The decrease in steepness of curve towards the tail end (post peak crack behavior of curve) in load-CMOD curve for smaller beams compared to larger beam indicates the transformation of the brittle behavior of larger beam that occur due to their unstable crack growth to the stable one for smaller beams which indicates their ductile behavior. As the steepness of post peak portion of the curve for the beams increases, their brittleness increases. The vice versa is also true i.e. as the flatness of the tail end of load-CMOD curve of small beam increases, the ductility of it increases and is identified by Frank Papworth [10]. Thus, the ductility of the beams increases as its size reduces.

The size independent initial fracture energy (G_f) of SFRSCC derived from experiments is 418.3 N/m whereas for SCC, it is about 86.33 N/m. For SFRSCC, it is about 4.85 times higher than that of SCC. However the G_f of SFRSCC by simulation was found to be 425.76 N/m which is slightly higher than that from experiments. This increase in (G_f) of SFRSCC is due to the presence of steel fibers in the SCC.

The higher values of fracture energies G_{FRC} and G_f of SFRSCC beams as compared to SCC are responsible to impart the toughness and ductility in smaller beams.

The fracture process length (c_f) for SFRSCC from experiments is about 88.45 mm whereas for SCC, it is about 18.72 mm, which is 4.725 times higher than that of SCC. However, its value from simulation is 115.23 mm which is higher as compared to experimental value. Substituting the higher value of c_f of SFRSCC beams in the brittleness number $\beta = \left(\frac{D*g\left(\frac{a_o}{D}\right)}{c_f*g'\left(\frac{a_o}{D}\right)}\right)$ given by Bazant and Khazemi, the β decreases. The greater the value of c_f of SFRSCC beams will reduce the value of brittleness number $\beta=\frac{(D}{D_o)}$. As β decreases, the ductility of SFRSCC beams increases.

The $CTOD_c$ for SFRSCC is found to be 0.0975mm where as for SCC, the average of three companion beams are 0.0146 mm, 0.0112mm and 0.00786 mm for L.P series, M.P series and S.P series respectively. However, the $CTOD_c$ determined by simulation is 0.110 mm which more than that of experimental value. Substituting the higher value of $CTOD_c$ of SFRSCC beams in the expression the material length "Q" given by $\left(\frac{E*CTOD_c}{K_{IC}}\right)^2$ where K_{IC} and $CTOD_c$ are fracture parameters that depends only on the material, the value of Q increases. As Q increases, the ductility of the SFRSCC beams increases. Hence SFRSCC beams are more ductile compared to SCC beams due to the higher value of $CTOD_c$.

VI.INVESTIGATION OF THE SIZE EFFECT IN SFRSCC BEAMS

To draw the size effect diagram, the peak loads of the experimental and simulation load CMOD curves are used to determine the respective G_f and c_f as per the RILEM test procedure. The corresponding constants such as characteristic size D_o and Bf_t for geometrically similar beams are determined by the relation suggested by Bazant and Kazemi in the size effect model (SEM) as $D_o = c_f\left[\frac{g'\left(\frac{a_o}{D}\right)}{g\left(\frac{a_o}{D}\right)}\right]$ and $Bf_t = c_n\,[\frac{EG_f}{[c_f g'\left(\frac{a_o}{D}\right)]}]^{0.50}$ where $g\left(\frac{a_o}{D}\right)$ and $g'\left(\frac{a_o}{D}\right)$ are the geometric factor and its derivative respectively for S/D ratio =4. For simply supported beam, the constant c_n=1.5 $\left(\frac{Span}{Depth}\right)$ = (1.5*4) = 6.00.

The nominal (failure) stresses σ_N are calculated in each beam size by the relation $\sigma_N = \left[\frac{Bf_t}{\sqrt{1+\left(\frac{D}{D_o}\right)}}\right]$ as derived in the size effect model (SEM) method. The D_o is a characteristic depth in geometrically similar beams at which the line representing both strength and LEFM criterion meet in the size effect diagram

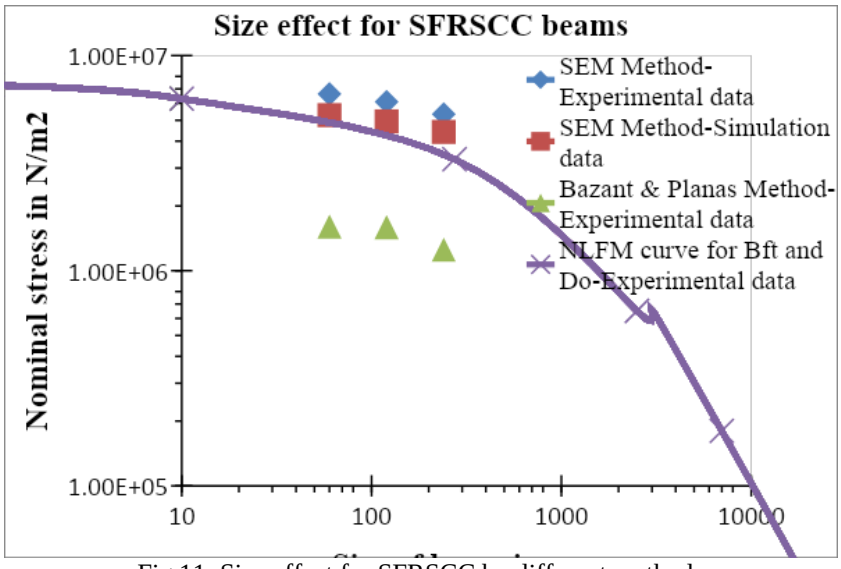

Fig 11: Size effect for SFRSCC by different methods

Alternatively, the method suggested to determine the size effect by Bazant and Planas [5] is ideally suitable for SFRSCC beams in which the crack zone behaves as plastic section. This method calculates σ_N by dividing the peak load by beam depth and width.

These are represented in the form of graph on logarithm scale as shown in **Fig 11** above.

It is evident from this graph that the size effect is almost negligible for SFRSCC beams of small and medium sizes since there is no appreciable difference in nominal stresses (σ_N) of these beams as compared to the larger beam. This is due to the large ammount of G_{FRC} experienced by smaller beams due to the presence of steel fibers. The fracture process zone of the smaller beams will be transformed into plastic section. Hence there will be no size effect in small beams. But the decrease in nominal stress as compared to these beams is noticeable only for larger sized beam of depth 240 mm. Hence there will be the size effect only in the larger SFRSCC beams.

VII. CRACK MODEL CHARACTERIZATION

The characterization of the softening curve from experimental load-CMOD curve is essential for the fracture behavior of SFRSCC beams. The crack model has to be developed for SFRSCC by linking it with the experimental fracture parameters. A typical softening law is to be established for SFRSCC.

TABLE 7
STRESS RATIO AT KINK POINT IN THE CRACK MODEL

Beam ID	Ultimate load P_U in kN	Load at kink point in kN	Ψ_1
L-F-1	20.205	18.30	0.906
L-F-2	20.09	18.22	0.907
L-F-3	19.45	17.81	0.916
M-F-1	13.02	11.19	0.860
M-F-2	12.80	11.25	0.879
M-F-3	12.75	10.98	0.861
S-F-1	6.53	5.51	0.844
S-F-2	6.43	5.55	0.863
S-F-3	6.415	5.53	0.862

The stress ratio Ψ_1 at the kink point 1 is obtained by taking the ratio of load at kink point to that of the ultimate load P_U for all the beams as given in **Table 7** above. From this table, it is observed that Ψ_1 is in the range from 0.844 to 0.916.

Due to the inclusion of discrete steel fibers, the FPZ of SFRSCC beam is different than that of SCC. Since the fiber bridging zone of nonlinear FPZ of SFRSCC represented by the ascending and descending slope at second kink point is larger as compared to its small range of aggregate bridging zone represented by portion before the first kink point as shown in **Fig 13** below, a large quantity of additional energy is required for de-bond and pull out of steel fibers from the SCC matrix. This is responsible to yield large values of fracture energies in SFRSCC beams and is also responsible to increase the ductility of these beams compared to SCC beams due to plastic behavior of crack zone in presence of steel fibers thereby extending the crack width at larger loads.

In case of SCC beams, there will be only aggregate bridging zone of smaller extent which is responsible for softening of the SCC in descending order.

The proposed softening model can be developed from the experimental Load CMOD curve for SFRSCC as shown in **Fig 12** below. Hence, it can be briefed by the following experimental fracture parameters of SFRSCC. These are as follows,

1. Tensile strength (f_t) is equivalent to the peak load of the load CMOD curve.
2. Total fracture energy (G_{FRC}) represented by the area under the entire softening curve.
3. Initial fracture energy G_f is the area under first slope represented by aggregate bridging zone of the softening model.
4. Stress ratio at first kink point (Ψ_1) as calculated from the procedure as above.
5. Hypothesizing, $w_{k2} = CTOD_c$ of SFRSCC,
6. Depth 'D' of the beam under consideration and the depth of maximum size (D_{max}) in a series of geometrically similar beams.

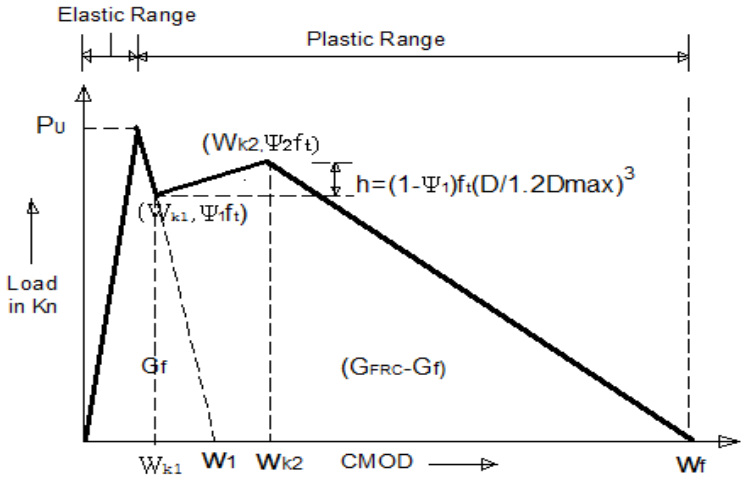

Fig 12:Load-CMOD curve for SFRSCC beams under 3-point loading

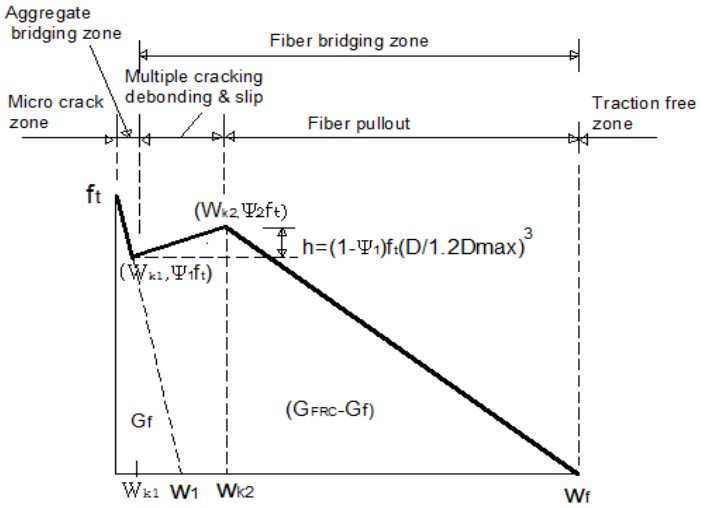

Fig 13: Characterization of crack model for SFRSCC beam

Referring to **Fig 13**, the co-ordinates of kink points are calculated as follows,

Equating the area under first slope of the curve, we have,

$G_f = \frac{1}{2} f_t w_1 \qquad \therefore w_1 = \left(\frac{2G_f}{f_t}\right)$ (5)

From similar triangles developed in this area, we have, $\left(\frac{w_1 - w_{k1}}{\Psi_1 f_t}\right) = \left(\frac{w_1}{f_t}\right)$

By rearranging the above equation, We have, $w_{k1} = (1-\Psi_1)w_1 = \left[(1-\Psi_1)\left(\frac{2G_f}{f_t}\right)\right]$ (6)

Thus the co-ordinate of the first kink point $(w_{k1}, \Psi_1 f_t)$ can be calculated.

Similarly, the co-ordinate of second kink point $(w_{k2}, \Psi_2 f_t)$ can be calculated as follows,

Hypothesizing, $w_{k2} = CTOD_c$ (7)

And using the value of Ψ_1, the expression for " h" can be empirically formed as

$h = (1-\Psi_1) f_t \left(\frac{D}{1.2D_{max}}\right)^3$ (8)

D is the depth of the beam under consideration and

D_{max} is the depth of the larger beam in a series of geometrically similar section in the model.

From above **Fig 10,** $\Psi_2 f_t = (\Psi_1 f_t + h) = [\Psi_1 f_t + (1-\Psi_1) f_t \left(\frac{D}{1.2D_{max}}\right)^3]$

$\Psi_2 f_t = [\Psi_1 + (1-\Psi_1)\left(\frac{D}{1.2D_{max}}\right)^3] f_t$ and $\Psi_2 = [\Psi_1 + (1-\Psi_1)\left(\frac{D}{1.2D_{max}}\right)^3]$ (9)

Thus, the coordinates of kink points $(w_{k1}, \Psi_1 f_t)$ and $(w_{k2}, \Psi_2 f_t)$ are evaluated.

Similarly, equating the area of final descending line of softening curve,

$$\left(G_{FRC} - G_f\right) =$$

$$\left\{\left[0.50 * (\Psi_1 f_t + h) * \left(w_f - w_{k2}\right)\right] + [0.50[(w_{k2} - w_1) + (w_{k2} - w_{k1})] * \Psi_1 f_t] + [0.50h * (w_{k2} - w_{k1})]\right\}$$ (10)

Substituting the value of $\Psi_1, w_{k2}, G_{FRC}, G_f$, D,$D_{max}, w_{k1}, w_1$ and f_t in the above equation (10), the value of w_f can be calculated.

VIII.MEASUREMENT OF TOUGHNESS

TABLE 8

ESTIMATION OF AREAS UNDER P-CMOD CURVES TO OBTAIN TOUGHNESS IN SFRSCC BEAMS

Beam	P_U **In kN**	w_u **in mm**	P_{cr} **In kN**	**δ at first crack in mm**	**Area of AOB in kN-mm**	**Area for I_5 in kN-mm**	**Area for I_{10} in kN-mm**	**Area for I_{30} in kN-mm**
L-F-1	20.205	0.135	11.12	0.0533	0.2970	2.1117	4.6290	14.5162
L-F-2	20.09	0.140	12.13	0.0587	0.3560	2.5063	5.4148	17.0168
L-F-3	19.45	0.142	11.59	0.0522	0.3025	2.0843	4.5164	14.1752
M-F-1	13.02	0.120	6.76	0.0413	0.1396	1.0122	2.2475	6.9981
M-F-2	12.80	0.118	6.67	0.0439	0.1435	1.0618	2.3504	7.3380
M-F-3	12.75	0.120	6.47	0.0418	0.1352	0.0984	2.1578	6.8614
S-F-1	6.530	0.092	3.33	0.0345	0.0575	0.4269	1.0030	3.4334
S-F-2	6.430	0.090	3.22	0.0312	0.0502	0.3802	0.9451	2.9303
S-F-3	6.415	0.086	3.13	0.0313	0.0470	0.3512	0.8932	2.7902

Using the experimental load CMOD curves, the toughness indexes I_5, I_{10} and I_{30} are calculated as per ASTM C1018 for all beams and presented in **Table 8** above and **Table-9** below.

Using experimental load-CMOD curves for L-F-1 beam as shown in **Fig 14** below, the toughness indices, toughness ratio R_{10-30} and average bending stress (f_{10-30}) are evaluated as follows,

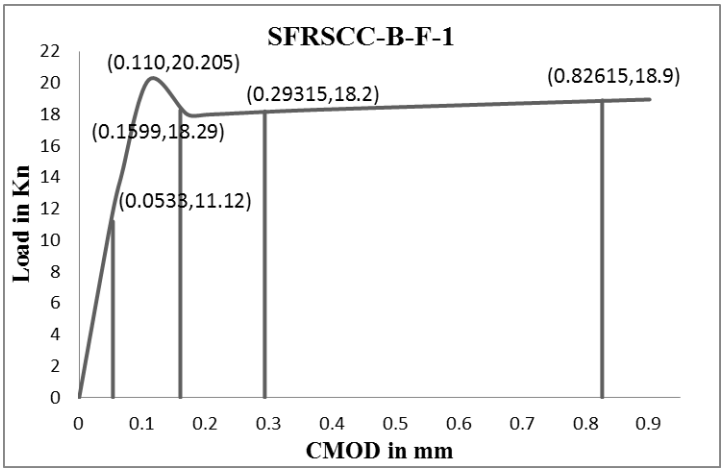

Fig 14: Co-ordinates of load-CMOD curves at different values of δ

From the above **Fig 14,** for steel fiber reinforced SCC specimen S-F-1,

We have, $I_5 = \left[\frac{Area\ of\ OACDBO\ \ for\ I_5 in\ kNmm\ at\ 3\delta}{Area\ of\ AOB\ in\ kNmm\ at\ first\ crack\ \delta}\right] = \left[\frac{2.1117}{0.297}\right] = 7.11$ (11a)

$I_{10} = \left[\frac{Area\ \ for\ I_{10} in\ kNmm\ at\ 5.5\delta}{Area\ of\ AOB\ in\ kNmm\ at\ first\ crack\ \delta}\right] = \left[\frac{4.6290}{0.297}\right] = 15.59$ (11b)

$I_{30} = \left[\frac{Area\ \ for\ I_{30} in\ kNmm\ at\ 15.5\delta}{Area\ of\ AOB\ in\ kNmm\ at\ first\ crack\ \delta}\right] = \left[\frac{14.5162}{0.297}\right] = 48.83$ (11c)

Av Bending stress$(f_{10} - f_{30}) = \frac{[(I_{30}-I_{10})}{(15.5\delta-5.5\delta)]}$

$= \left[\frac{(48.83-15.590)}{10X0.0533}\right] = 62.46\ MPa$ (12)

Toughness Ratio $(R_{10-30}) = \left[\frac{(I_{30}-I_{10})_{SFRSCC}}{(I_{30}-I_{10})_{EP}}\right] * 100$

$= 5(I_{30} - I_{10}) = 5(48.83 - 15.59) = 166.45\ \%$ (13)

Toughness Ratio $(R_{10-30}) = \left(\frac{(f_{10}-f_{30})}{f_o}\right) * 100$ (14)

Where $f_o = \frac{[(I_{30}-I_{10})}{(15.5\delta-5.5\delta)]_{EP}} = \left(\frac{20}{10\delta}\right) = \left(\frac{2}{\delta}\right)$ (15)

By rearranging the above toughness ratio equation, we have,

$Av\ bending\ stres = \frac{[f_o(R_{10-30})]}{100} = \left[\left(\frac{2}{\delta}\right) X \frac{(R_{10-30})}{100}\right] = \left[\left(\frac{2}{0.0533}\right) * \left(\frac{166.45}{100}\right)\right] = 62.46MPa$ (16)

These values are calculated for the remaining beams and are presented in **Table 9** below,

TABLE 9
CALCULATION OF TOUGHNESS INDEX FOR SFRSCC BEAMS

Beam ID	I_5	I_{10}	I_{30}	**Av Bending Stress** $(f_{10} - f_{30})$	$(f_{10} - f_{30})_e$	**Toughness Ratio**(R_{10-30})	$(R_{10-30})_e$
L-F-1	7.11	15.59	48.83	62.46	58.96	166.45	161.53
L-F-2	7.04	15.21	47.80	55.52		162.95	
L-F-3	6.89	14.93	46.86	61.17		159.65	
M-F-1	7.25	16.10	50.13	82.40	81.70	170.15	181.00
M-F-2	7.40	16.38	51.14	83.16		173.80	
M-F-3	7.28	15.96	50.75	83.23		173.95	
S-F-1	7.43	17.45	59.76	122.64	119.16	211.55	194.11
S-F-2	7.58	18.84	58.26	126.35		197.10	
S-F-3	7.48	19.02	59.43	129.11		202.05	

The results given in **Table 9** are used to develop the graphs showing the variation of average bending stress in **Fig 15** and variation of toughness ratio with respect to size of beam as shown in **Fig 16** below.

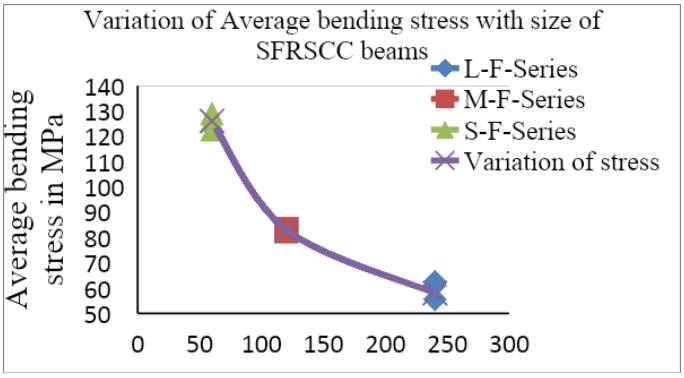

Fig 15: Graph showing the variation of average bending stress v/s size of beam

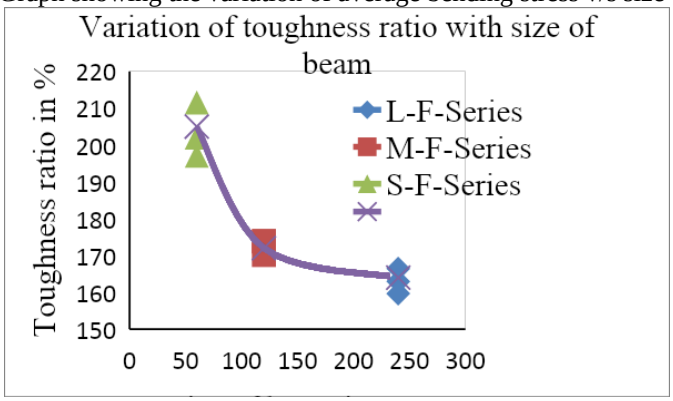

Fig 16: Graph showing the variation of toughness ratio v/s size of beam

From the results given in above **Table 9**, it is learnt that there is a systematic increase in the index values I_5, I_{10}, I_{30}, average bending stresses and toughness ratios as the size of the notched beam decreases and are considered to be size dependent. The average bending stress is higher for smaller beams. Thus the maximum ultimate design moment given by $M_{ult} = \left[\frac{(f_{10-30})Z}{\gamma_m}\right]$ for smaller beams increases where Z is the section modulus and γ_m is the factor of safety whose value is taken as 1.20.

The empirical relations can be established for average bending stress $(f_{10} - f_{30})_e$ and toughness ratio $(R_{10-30})_e$ in terms of the size of beam D as follows,

$$(f_{10} - f_{30})_e = \left[\frac{125}{1+(\frac{D}{200})^{\frac{150}{D}}}\right] \quad \text{And} \quad (R_{10-30})_e = \left[\frac{210}{\sqrt{1+\frac{D}{350}}}\right] \qquad (17)$$

The numerical values calculated from these empirical equations are given in above **Table 9**.

Determination of the Ductility Ratio

The experimental load CMOD curves shown in **Fig 6** are used to determine the member ductility ratio (μ_m) of beams and these values are represented in **Table 10** below.

TABLE 10
DETERMINATION OF DUCTILITY RATIOS

Beam ID	From experimental load CMOD curves						From simulation curves				
	P_U in kN	P_y in kN	U_y in mm	U_{max} in mm	μ_m	$(\mu_m)_e$	P_U in kN	P_y in kN	U_y in mm	U_{max} in mm	μ_m
L-F-1	20.21	18.30	0.30	1.18	3.93	3.96	18.80	17.50	0.43	1.92	4.67
L-F-2	20.09	18.22	0.29	1.25	4.31						
L-F-3	19.45	17.81	0.29	1.28	4.42						
M-F-1	13.00	11.19	0.25	1.32	5.28	5.36	11.01	10.60	0.32	2.05	6.40
M-F-2	12.80	11.25	0.24	1.30	5.42						
M-F-3	12.75	10.98	0.23	1.24	5.39						
S-F-1	6.53	5.51	0.20	1.43	7.15	7.21	5.46	5.18	0.26	2.21	8.50
S-F-2	6.43	5.55	0.19	1.55	8.15						
S-F-3	6.42	5.53	0.20	1.52	7.60						

A graph is developed in **Fig 17** showing the variation of member ductility ratio with size. Its value usually varies less than 10.

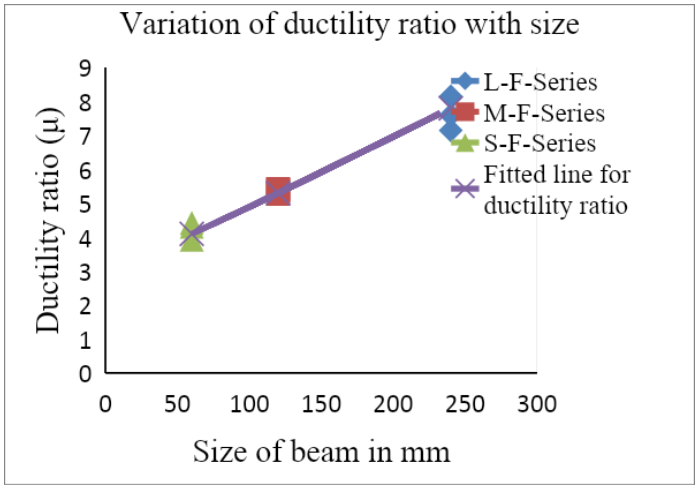

Fig 17: Graph showing the variation of ductility ratios (μ) with size of beam

The member ductility ratio (μ_m) is size dependent property. As the size of beam increases, its value increases. For any intermediate size above 60 mm, it can be determined using an equation for linear regression line as in expression (18) or an empirical formula as established in expression (19) below.

$$Ductility\ ratio(\mu_m) = \left[4.1 + \frac{(7.8-4.1)*(D-60)}{180}\right] = [4.1 + 0.0206 * (D - 60)] \quad (18)$$

$$Empirical\ expression\ for\ Ductility\ ratio(\mu_m)_e = \left\{\frac{7.5}{[1+(\frac{D}{300})^{\frac{120}{D}}]}\right\} \quad (19)$$ where D is in mm

The structural ductility factor (μ_b) for the framed building should be determined using the pushover analysis. Its quantification requires a relationship between lateral loads and displacement of whole building which is beyond the scope of present study. An attempt can be made later to establish an equation for (μ_b) in terms of (μ_m) for multistoried framed building frame because the structural ductility depends on member displacement ductility. For single storey frame, the relationship between μ_m and μ_b is expressed in terms of the ratio of member stiffness of beam and column. Using (μ_b), an empirical expression for R can later be studied. Attempts are made to express R by an empirical expression given by $R = \sqrt{\mu^{1.5} - 1}$ (20)

However, further study is required to re-affirm this empirical equation.

CONCLUSIONS

- Since the simulated load CMOD curves will provide a better fit with the experimental load CMOD curves, the experimental fracture parameters are useful to predict the tri-linear crack model by simulation using ATENA software with smeared crack approach which is based on Bazant's crack band model. Hence a tri-linear crack model can be developed for SFRSCC by linking its fracture parameters.
- The ductility increases with decrease in beam sizes. The decrease in peak loads of smaller beams associated with their high fracture energies will increase the characteristic length (L_{ch}) which indicates the increase in ductility. The ductility is also measured by ductility ratio (μ). It increases as the size of beam decreases and is the size dependent property. An empirical formula expressed for ductility ratio (μ_m) is introduced in terms of size of beam. This value of μ estimated for any intermediate size is useful to determine the response reduction factor (R) by empirical expression $R = \sqrt{\mu^{1.5} - 1}$ which is introduced to consider ductility in base shear formula of I.S.1893 code used for design of earthquake resistant buildings. The empirical formulas established for μ and (R) are useful for design of SFRSCC structures considering ductility property.
- The higher values of fracture energies G_{FRC} and G_f of SFRSCC beams as compared to SCC are responsible to increase their toughness and ductility. The higher value of $CTOD_c$ of SFRSCC beams compared to SCC beams is also responsible to increase the ductility of these beams since $CTOD_c$ is responsible to increase the material length "Q". As Q increases, the ductility of the beams increases. The greater the value of c_f of SFRSCC beams will reduce the value of brittleness number β=$\frac{(D}{D_o)}$. As β decreases, the ductility of SFRSCC beams increases.
- The higher values of fracture energies G_{FRC} in small size beams compared to larger beams will transform the fracture process zone (FPZ) of the beam to behave like a plastic section there by absorbing large amount of energy. This will reduce the size effect in SFRSCC beams of smaller size. However, the size effect is noticeable only in larger size beam.
- The average values of the toughness indexes, average bending stress f_{30-10} and toughness ratio R_{30-10} increases systematically as the size of the member decreases. Empirical expressions established for these values

in terms of the size of the beam are useful for the design of structures based on toughness.

ACKNOWLEDGEMENTS

The author sincerely thanks the management and principal of Smt. Kamala and Shri. Venkappa. M. Agadi College of Engineering and Technology (SKSVMACET) LAXMESHWAR --582116, Dist: Gadag, Karnataka State for the support and encouragement given throughout the course of this work.

NOTATIONS

The following symbols are used in this paper.

L-F-1,2,3	Large size-Fiber-Beam specimen no 1,2 and 3 respectively
M-F-1,2,3	Medium size-Fiber-Beam specimen no 1,2 and 3 respectively
S-F-1,2,3	Small size-Fiber-Beam specimen no 1,2 and 3 respectively
L-P series	Larger size-Plain SCC Beam series
M-P series	Medium size-Plain SCC Beam series
S-P series	Smaller size-Plain SCC Beam series

REFERENCES

1. Hillerborg," Analysis of fracture by means of the fictitious crack model, particularly for fiber reinforced concrete" The international Journal of Cement Composites,Volume-2,No-4,(1980),pp177-184.
2. K. Visalvanich and A.E.Naaman,"Fracture model for Fiber reinforced Concrete" ACI Materials Journal, No 80-14,(1983),pp 128-138
3. Jun, Zhang., and Victor, C, Li., "Simulation of crack propagation in fiber reinforced concrete by fracture mechanics" Cement and Concrete Research ,Volume 34,(2004), pp 333-339.
4. Jeffery,Roesler.,Glaucio,H.,Paulino,Kyoungsoo, Park., and Cristian Gaedick."Cohesive Fracture Model for functionally graded fiber reinforced concrete", Cement and Concrete Research, Volume-40, March-(2010), pp 956—965.
5. Jeffery, Roesler., Glaucio.H.Paulino., Kyoungsoo, Park. and Cristian, Gaedick., "Concrete fracture prediction using bilinear softening", Cement and Concrete Composites, Volume -29, (2007), pp. 300--312.
6. JefferyRoesler, Glaucio.H.Paulino, Kyoungsoo Park and CristianGaedick ,Determination of the kink point in the bilinear softening model for concrete, Engineering fracture mechanics, Volume No-75, (2008), pp. 3806--3818.
7. V.S.Gopalkrishnan., and S.P.Shah., "Tensile failure of steel fiber reinforced mortar", Journal of engineering mechanics-ASCE113 (5)-(1987), pp. 635-652.
8. Cervenka, V., and Pukl, R., "Sbeta analysis of size effect in concrete Structures", Proceedings of the second international conference on fracture mechanics of concrete structures, (FRAMCOS2):1387-1396, Ed.F.H.Wittmann, AEDIFICATIO, ETH Zurich, (1995), Switzerland.
9. Apparao,G.,and Raghuprasad,B.K., "Fracture energy of fiber reinforced high strength concrete", Journal of Structural Engineering, SERC ,Chennai, Volume-31,No-4, January-March (2005), pp. 249-255.
10. Frank, Papworth. "Use of steel fibers in concrete", Presented at the Concrete Institute of Australia, NSW branch (1997), pp 1–10.
11. Perumalsamy, N, Balaguru., A text book "Fiber reinforced cement composites" McGraw Hill Inc, ISBN 0-07-112967-7, International edition (1992), pp. 149-150,482.
12. Joe, Nasvik., "Increasing concrete durability– what happens when you add steel fibers to concrete", Concrete Construction, April– (2012).
13. Pankaj, Agarwal, and Manish Shrikhade "A text book on "Earthquake resistant design of structures" PHI Publishers, New Dehli, ISBN-81-203-2892-2, Edition-September (2006) ,pp. 243,252-254,342-343.
14. H. Vijayakumar., and Sakey, Shamu., "A critical study on the influence of steel fiber on performance of fresh and hard self-compacting concrete" Journal of structural engineering, SERC ,Chennai, Volume-42,No-3, August -September (2015), pp. 237-245.
15. Nan, Su, Hsu, K.C., and Chai, H.W., "A simple mix design for self–compacting concrete", Cement and concrete Research, Volume 31(2001), pp1799–1807.
16. Shah.S.P., Swartz.S.E and Ouyang.C, A text book on fracture mechanics of concrete: application of fracture mechanics to concrete, rock other quasi-brittle material. Published by John Wiley and Sons, pp-211.
17. H.Vijayakumar and Sakey shamu., Published "Fracture model prediction for self-compacting concrete using bi-linear softening" The international reviewer(ISSN 2395-1575),Volume 4,Issue 2,July- December 2017,pp.29-34.

ABOUT THE AUTHOR

Dr. Vijayakumar. Halakatti *is awarded PhD degree from VTU Belgaum, Karnataka state, India in the year 2018.He completed M.E (structures) from Gulbarga University and B.E (civil) from Karnataka University Dharwad .He has more than 27 years of teaching experience at undergraduate level as Lecturer, Senior Lecturer and Assistant Professor and Associate Professor at various colleges and universities in India. Presently he is working as Associate Professor, Department of Civil Engineering, SKSVMA Charitable Trust's Smt. Kamala and Shri. Venkappa. M. Agadi College of Engineering and Technology (SKSVMACET) LAKSHMESHWAR-582116 Dist: Gadag, Karnataka State, India. His areas of interest are finite element analysis and fracture mechanics of concrete and self-compacting concrete etc.*